Vasculostatin Inhibits Intracranial Glioma Growth and Negatively Regulates *In vivo* Angiogenesis through a CD36-Dependent Mechanism

Balveen Kaur,[1] Sarah M. Cork,[1] Eric M. Sandberg,[1] Narra S. Devi,[1] Zhaobin Zhang,[1] Philip A. Klenotic,[6] Maria Febbraio,[6] Hyunsuk Shim,[3,4,5] Hui Mao,[4,5] Carol Tucker-Burden,[2] Roy L. Silverstein,[6] Daniel J. Brat,[2,5] Jeffrey J. Olson,[1,5] and Erwin G. Van Meir[1,3,5]

Laboratory of Molecular Neuro-Oncology, Departments of [1]Neurosurgery, [2]Pathology, [3]Hematology/Oncology, and [4]Radiology, and [5]Winship Cancer Institute, Emory University, School of Medicine, Atlanta, Georgia; and [6]Department of Cell Biology, Lerner Research Institute, The Cleveland Clinic, Cleveland, Ohio

Abstract

Angiogenesis is a critical physiologic process that is appropriated during tumorigenesis. Little is known about how this process is specifically regulated in the brain. Brain angiogenesis inhibitor-1 (BAI1) is a brain-predominant seven-transmembrane protein that contains five antiangiogenic thrombospondin type-1 repeats (TSR). We recently showed that BAI1 is cleaved at a conserved proteolytic cleavage site releasing a soluble, 120 kDa antiangiogenic factor called vasculostatin (Vstat120). Vstat120 has been shown to inhibit *in vitro* angiogenesis and suppress subcutaneous tumor growth. Here, we examine its effect on the intracranial growth of malignant gliomas and further study its antitumor mechanism. First, we show that expression of Vstat120 strongly suppresses the intracranial growth of malignant gliomas, even in the presence of the strong proangiogenic stimulus mediated by the oncoprotein epidermal growth factor receptor variant III (EGFRvIII). This tumor-suppressive effect is accompanied by a decrease in tumor vascular density, suggesting a potent antiangiogenic effect in the brain. Second, and consistent with this interpretation, we find that treatment with Vstat120 reduces the migration of cultured microvascular endothelial cells *in vitro* and inhibits corneal angiogenesis *in vivo*. Third, we show that these antivascular effects critically depend on the presence of the cell surface receptor CD36 on endothelial cells *in vitro* and *in vivo*, supporting the role of Vstat120 TSRs in mediating these effects. These results advance the understanding of brain-specific angiogenic regulation, and suggest that Vstat120 has therapeutic potential in the treatment of brain tumors and other intracerebral vasculopathies. [Cancer Res 2009;69(3):1212–20]

Introduction

The process of angiogenesis is tightly regulated in normal adult tissues by maintaining a delicate balance between proangiogenic and antiangiogenic factors. In neoplasia, this balance is tilted in favor of new blood vessel development, thereby increasing its vascular supply and promoting growth and metastasis (1, 2). The production of proangiogenic molecules, such as vascular endothelial growth factor and interleukin 8 is increased, and the expression of antiangiogenic factors, such as thrombospondin-1 (TSP-1) is reduced (3, 4). Arresting angiogenesis in combination with other agents is currently being exploited as an effective new therapeutic modality for cancer (5, 6). Little is known about how physiologic angiogenesis is regulated in the brain and how it becomes co-opted during brain tumor development.

Gliomas are the most common primary tumor of the central nervous system. Glioblastoma (GBM), the most aggressive form of malignant astrocytoma (WHO grade 4) is characterized pathologically by a highly abnormal vasculature (7). During astrocytoma progression from low to high grade, increased vessel density coincides with malignant progression as well as an accumulation of genetic defects. The two genetic alterations that occur at the transition to WHO grade 4 GBM are the loss of the *PTEN* tumor suppressor gene and the amplification of the epidermal growth factor receptor (*EGFR*) proto-oncogene (8, 9). Apart from gene amplification and receptor overexpression, the *EGFR* gene is also frequently mutated in GBM. The most common of these mutations results in a truncated ligand-independent EGFRvIII with constitutive activity (10, 11). Importantly, both these events are known to increase the angiogenic phenotype of glioma cells.

Brain angiogenesis inhibitor-1 (BAI1) is a member of the "adhesion" subfamily of G protein–coupled receptors, thought to be involved in cell-cell and cell-matrix interactions (12, 13). Its expression is reduced in malignant gliomas, pulmonary adenocarcinoma, pancreatic and gastric cancers, but present in the corresponding normal tissue with, by far, the most abundant expression in the brain (14–16). Re-expression of BAI1 in tumor cells which have lost its expression has been shown to result in slow-growing tumors with reduced vessel density, suggesting an antiangiogenic function (17, 18). We recently described vasculostatin, a naturally occurring 120 kDa fragment (Vstat120) of BAI1 (19). We have shown that Vstat120 is released from BAI1 by proteolytic cleavage at a consensus G protein coupled receptor proteolytic cleavage site located close to the junction with the plasma membrane. Vstat120 contains an arginine-glycine-aspartate (RGD) integrin recognition motif and five thrombospondin type-1 repeats (TSR); both of these

Note: Supplementary data for this article are available at Cancer Research Online (http://cancerres.aacrjournals.org/).

Current address for B. Kaur: Dardinger Laboratory of Neuro-oncology and Neurosciences, James Comprehensive Cancer Center, Department of Neurological Surgery, The Ohio State University, Columbus, OH 43210.

Individual author contributions are specified in Supplemantary data.

Requests for reprints: Erwin G. Van Meir, Winship Cancer Institute, Emory University School of Medicine, 1365C Clifton Road Northeast, C5078, Atlanta, GA 30322. Phone: 404-778-5563; Fax: 404-778-5550; E-mail: evanmei@emory.edu.

doi:10.1158/0008-5472.CAN-08-1166

domains are known to mediate antiangiogenic functions in thrombospondins (20–22). However, it is not clear if the five TSRs contribute to the angiostatic effect of Vstat120.

We have shown that Vstat120 can suppress the growth of glial tumors in a subcutaneous mouse xenograft model (19). However, tumor growth as well as its response to targeted treatments is affected by its location and microenvironment (23). Despite its primarily brain-specific expression, the effect of Vstat120 on the growth of intracerebral tumors has not been investigated (13, 24). Here, we examined the effects of Vstat120 on the growth of gliomas of varying genetic makeup, degree of malignancy, and proangiogenic potential in their orthotopic environment. We have further investigated the antiangiogenic effects of Vstat120 in a number of *in vivo* and *in vitro* angiogenesis models and established that Vstat120 binding to CD36, an endothelial cell receptor for the TSR domains of TSP-1 and TSP-2, is essential for its angiostatic effect. These results indicate the functional significance of the five TSRs in Vstat120.

Materials and Methods

Culture of cell lines and transfection conditions. The human glioblastoma LN229 and embryonic 293 cell lines have been previously described (25). Two U87MG glioblastoma cell lines maintained independently in two laboratories were used. U87MG-D cells were provided to us by Dr. D. Durden's laboratory (Emory University, Atlanta, GA) and were used to derive the U87MGD-Vstat120 (clones U14 and U18) by stable transfection with an expression vector for Vstat120 (pcDNA3.1mychisVstat120). U87MG-F were obtained from Dr. F. Furnari's laboratory (Ludwig Institute for Cancer Research, La Jolla, CA) and were used to generate U87ΔEGFR cells which stably express the EGFRvIII mutant form of EGFR (26). U87MGD display more aggressive *in vivo* growth than U87MGF. The U87MGF-ΔEGFR-Vstat120 (clones Δ19 and Δ22) cells were prepared by stably transfecting U87MGF-ΔEGFR parental cells with pcDNA3.1mychisVstat120. The LN229Vstat120 (clone 13) and LN229TSP1 (clone C9) cells were prepared by stably transfecting LN229 cells with expression vectors for Vstat120 (pcDNA3.1mychisVstat120) and TSP-1 (pcDNATS1). Conditioned media (CM) were prepared from 80% confluent cultures grown for 48 to 96 h in serum-free medium. 293 cells were transiently transfected with the indicated plasmids using GenePORTER transfection reagent (Gene Therapy Systems) as recommended. Serum-free CM was collected from cells after 48 h and precipitated using 50% TCA as described (19). The primary cultures of endothelial cells [human umbilical vein endothelial cells (HUVEC) or human dermal microvascular endothelial cells (HDMEC)] were prepared by the Emory University Dermatology Core Facility and grown as described (19). Primary human brain (cortex; 24 year old) microvascular endothelial cells were purchased from Cell Systems Corp. (ACBRI376) and grown as recommended.

Preparation of recombinant glutathione-S-transferase fusion proteins. Two different glutathione-S-transferase (GST)/CD36 constructs containing the CLESH domain (spanning amino acids 5–143 and 67–157) were prepared as previously described (27). The GST fusion proteins were expressed in *Escherichia coli* Bl21(DE3) bacteria, induced at log phase with 3 mmol/L of IPTG for 3 h at 37°C. The bacteria were centrifuged and resuspended in 5 mL of lysis buffer [PBS, One Complete mini EDTA-free protease inhibitor cocktail tablet (Roche), and 1 mg/mL lysozyme] and frozen overnight at −20°C. The bacterial solutions were thawed in warm water and pulse-sonicated (3 × 15 s). Lysates were sedimented at 31,000 × *g* for 30 min, followed by successive washes with buffer 1 (25 mL of PBS, 0.1% Triton X-100), and buffer 2 (50 mmol/L NaH_2PO_4, 300 mmol/L NaCl; pH 8.0), and dissolved in 5 mL of denaturing buffer (8 mol/L urea, 50 mmol/L Tris-HCl; pH 8.0). After 30 min of centrifugation at 30,000 × *g* to remove insoluble debris, the proteins were refolded by drop-wise addition into 20 mL of refolding buffer (50 mmol/L Tris-HCl, 1 mmol/L DTT, 1 mmol/L EDTA; pH 9.0), then dialyzed overnight in 50 mmol/L Tris (pH 8.0). Recombinant proteins bound to glutathione sepharose 4B resin (GE Healthcare) were either purified by elution with 50 mmol/L of Tris-HCl, 10 mmol/L of glutathione or used to pull down Vstat120 or TSP-1.

GST pull-down assay. The GST-CD36-CLESH fusion protein solutions (15 mL) were preabsorbed with 100 μL of glutathione sepharose 4B beads (GE Healthcare) for 2 h at 4°C. After two washes with cold PBS, 15 mL of undiluted CM (collected after 96 h in serum-free medium) from stably transfected or parental control cells was added to 100 μL of beads at 4°C overnight with constant rotation. The beads were centrifuged (100 × *g* for 1 min) and washed twice with 5 mL of PBS. Bound proteins were eluted and solubilized in 50 μL of SDS-PAGE denaturing sample buffer.

Western blot analysis. Immunoblots were performed on cell lysates (lysed in 8 mol/L urea, 4% SDS, in 10 mmol/L Tris; pH 7.4), from the indicated cells or tissue. Protein lysates (40 μg) were resolved on 7.5% SDS-PAGE and Western blots probed with rabbit anti–NH_2-terminal BAI1 (14), or goat anti-actin (diluted 1:500; Santa Cruz Biotechnology, Inc.) or anti-GST antibodies (MAB3317; Chemicon International), followed by goat anti-rabbit (DAKO, Co.) or swine anti-goat (diluted 1:1,000; Roche Molecular Biochemicals) secondary antibodies, and visualized by enhanced chemiluminescence (Pierce).

Proliferation assays. Proliferation rates of the different Vstat120-transfected and empty vector clones was assessed by the crystal violet assay (28). Equal cell numbers (4,000) of the indicated clones were plated in 96-well plates ($n = 8$). The cells were fixed with 1% glutaraldehyde, and then stained with 0.5% crystal violet. After washing, the crystals were dissolved in Sorenson's buffer (0.025 mol/L sodium citrate, 0.025 mol/L citric acid in 50% ethanol) and absorbance was read at A_{590} nm.

Tumorigenicity studies. Subcutaneous tumor xenografts were performed as previously described on mice marked by tattoos for identification (19, 29). To establish orthotopic brain tumor xenografts, 10^6 glioma cells were stereotactically injected into the brains of athymic nu/nu rats as described (30). Animals were anesthetized by i.p. injection of ketamine (80 mg/kg)/xylazine (10 mg/kg) mixture and then secured to a stereotactic frame. Body temperature was maintained by a heating pad. A saggital midline incision was made from 5 mm anterior to the bregma to the occiput. A 2-mm drill was then used to make a burr hole 3 mm to the right and 1 mm anterior of the bregma of the skull. A 23-gauge Hamilton syringe was advanced 4.5 mm deep over a period of 1 min, and then retracted 0.5 mm prior to injecting 5 μL of tumor cell suspension over a period of 2 min. Postinjection, the needle was slowly retracted over a period of 1 min, the burr hole filled with sterile bone wax, the skull washed with sterile water to destroy, by osmosis, any cells leaked into the subgaleal space and the scalp was closed with 3–0 running vicryl stitches. Survival curves were compared using the log-rank test using SPSS statistical software (version 14.0; SPSS, Inc.) and $P < 0.05$ values were considered significant. Studies followed Emory University Institutional Animal Care and Use Committee guidelines.

Magnetic resonance imaging. Magnetic resonance imaging (MRI) scans were carried out on a 3T MRI scanner (Philips Intera) using a small volume coil (5 cm diameter). Anesthetized animals were placed in the coil and the head secured using foam padding to minimize possible motions. MRI contrast agent, gadolinium diethylenetriamine-pentaacetic acid (Gd-DTPA), was administrated i.v. at a dose of 0.2 mmol/kg to obtain signal enhancement in the tumor. Multi-slice T1-weighted spin echo images were obtained in the coronal orientation using a repetition time of 400 ms, echo time of 14 ms, and imaging matrix of 128 × 128 with the field of view of 50 × 50 mm^2. To match the histologic analysis, a slice thickness of 2 mm was used without slice gap. The number of signal averages was three for most of the scans. T1-weighted spin echo imaging was done before and after administration of the contrast agent for each animal using the same imaging variables.

Histologic analysis. Tumors were fixed in 10% buffered formalin followed by paraffin embedding and immunohistochemistry of tissue sections (8 μm) to visualize the endothelial cells lining the blood vessels perfusing the tumor. The number of vascular structures/mm^2 in the tumor xenografts was quantified by counting three different 10× microscopic fields for each of three rats/group. The three fields were averaged in each tumor and the averages for each animal used to give the final count ± SE.

***In vitro* transwell and scratch-wound endothelial cell migration assays.** CM from HEK 293 cells transfected with Vstat120 (pcDNAecBAI1-myc-his) or control vector (pcDNA3.1-LacZ, a β-galactosidase expression vector) was collected and concentrated 40× using a YM-10 filter (Amicon). For the modified Boyden chamber migration assays, indicated cells were plated in transwell chambers (Becton Dickinson Labware) with a pore size of 8 μm (50,000 cells/chamber). The cells were placed on 1% serum-containing medium overnight and were then pretreated with CM (diluted at 1× in endothelial medium) for 30 min. Medium containing 10% serum was used as a chemoattractant in the bottom chamber, whereas CM remained in the upper chamber. After 8 h, migrated cells were quantified by counting three 10× microscopic views/filter and the data presented as the mean of three filters. Random migration in response to medium alone was subtracted from the values. For scratch-wound migration assays, confluent HDMECs were incubated in 1% medium overnight in 12-well plates, then wounded with a 10 μL pipette tip and detached cells were removed by PBS washes. The cells were treated with CM at a final concentration of 1× for 30 min with or without an anti-CD36 function–blocking antibody at 10 μg/mL (FA6-152; Cell Sciences), followed by incubation in 10% serum to induce cell migration. Initial wound width was measured, and the cells were allowed to migrate for 8 h, and were then fixed with 1% glutaraldehyde, stained with 0.5% crystal violet, and photographed. The experiment was repeated independently twice and significance determined by Student's *t* test.

***In vivo* cornea angiogenesis assays.** Pellets were generated as previously described (31) by mixing sterile solutions of basic fibroblast growth factor (bFGF; Research Diagnostics, Inc.) at a final concentration of 25 ng/pellet, concentrated CM (50 ng total protein from CM per pellet), and sucralfate (Teva Pharmaceuticals), and then spreading the solution onto a nylon mesh 3-300/50 with an approximate pore size of 0.4 × 0.4 mm (Tetko). The mixture was sealed on both sides with hydron. In this case, 7.5 μL concentrated medium/100 pellets were added. Individual pellets were detached by peeling the nylon mesh, and pellets of similar size were chosen under a dissecting microscope for implantation. Mice were anesthetized as above and the eyes were topically anesthetized with 0.5% proparacaine and 2% alocril and the globes proptosed with a forceps. Pellets were implanted ~1 mm from the limbus. Briefly, under a dissecting microscope, a central, intrastromal linear keratotomy (~0.5 mm in length) was performed with a surgical blade (Bard-Parker; Becton Dickinson), and using the arm of a fine forceps, a micropocket was created toward the limbus. Pellets were placed at the base of the pocket. Erythromycin antibiotic ointment was applied to the operated eye, both to prevent infection and to decrease irritation. Mice received Buprenex (2.5 mg/kg s.c.) after surgery to control for pain. Five days postimplantation, mice were anesthetized and 50 μL of a 2.5 mg/mL solution of sterile FITC-dextran (molecular weight approximately M_r 70,000; Sigma) was injected into the retro-orbital sinus. The eyes were proptosed as before, and digital images of the cornea were captured under a fluorescent dissecting microscope (Leica) and transferred to Adobe Photoshop for measurements. The maximum vessel length and the neovascularization zone (in clock hours), were used to calculate the area of neovascularization, using the formula: area (mm^2) = 0.2 × π × VL (mm) × CH; VL, vessel length; CH, clock hours; where one clock hour equals 30 degrees of an arc.

Results

Expression of Vstat120 suppresses the growth of intracranial gliomas. Because BAI1 is predominantly expressed in the brain, we investigated the role of its proteolytic cleavage product, Vstat120, on the orthotopic growth of brain tumors. We first generated two clones (U14 and U18) expressing and secreting Vstat120 in human U87MGD malignant glioma cells following stable transfection with an expression vector (Fig. 1*A*). The *in vitro* proliferation rates of these cells were not altered by Vstat120 expression (Fig. 1*B*). We confirmed that CM from Vstat120-expressing cells significantly inhibited the migration of HDMEC (Fig. 1*C*), as we previously described (19). To assess the therapeutic potential of Vstat120 expression on tumor growth in the brain, we implanted U14, U18, and parental U87MGD cells (10^6/animal) stereotactically into the brains of athymic nude rats (n = 6 rats/group). Both Vstat120-expressing clones extended the median survival of animals compared with the control parental U87MGD cells (P < 0.05). The median survival of animals injected with control parental

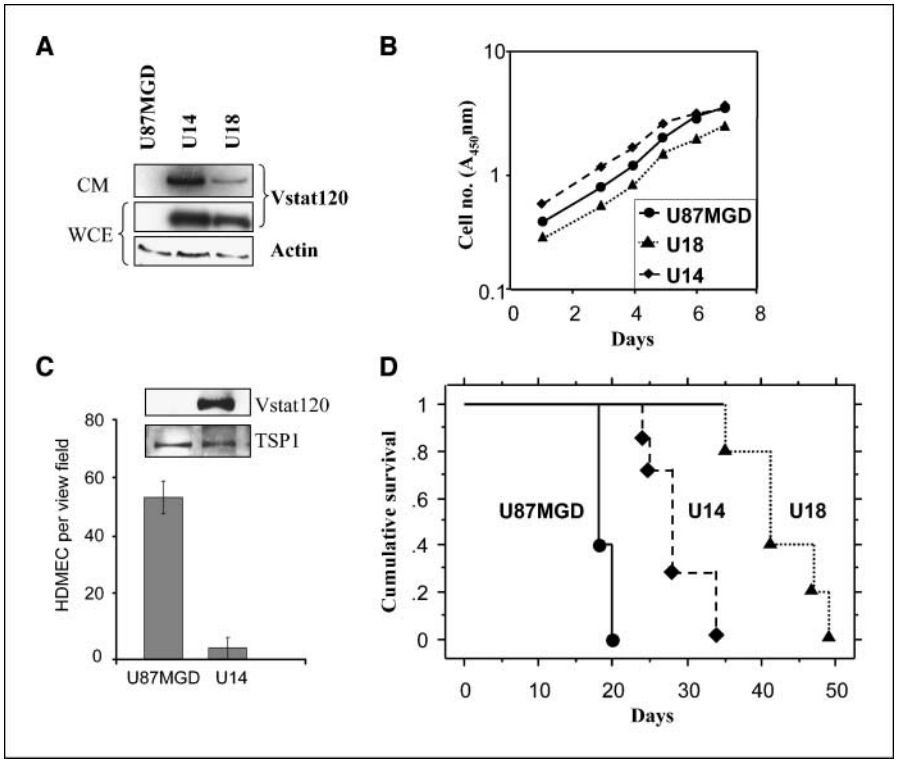

Figure 1. Expression of Vstat120 enhances the survival of rats implanted with U87MGD glioma cells in the brain. *A,* Western blot analysis of cell lysates from U87MG parental cells and U87MG-derived clones stably transfected with Vstat120 cDNA (*U14* and *U18*). Note the expression of Vstat120 in the whole cell extract (*WCE*) and conditioned medium (*CM*) of the stably transfected clones. *B,* the *in vitro* proliferation rates of U87MG cells and clones U14 and U18 were determined by the crystal violet assay. Expression of Vstat120 did not alter the proliferation rate of the clones versus U87MG cells. *C,* CM from control U87MGD or Vstat120-expressing U14 cells were tested for their ability to inhibit the migration of HDMECs in a transwell migration assay. The number of cells that migrated to the bottom of the chamber after 8 h was quantified as described in Materials and Methods. Random migration in response to medium alone was subtracted from the values. Expression levels of Vstat120 and TSP-1 in the CM were assessed by Western blot. *D,* intracranial tumorigenicity assay for U87MG and Vstat120-expressing clones, U14 and U18. Cells (1×10^6) were implanted stereotactically in the brain of athymic nude rats. Survival curves of rats implanted with cells expressing Vstat120 showed a significant improvement in their survival compared with the control parental U87MG cells (P < 0.05).

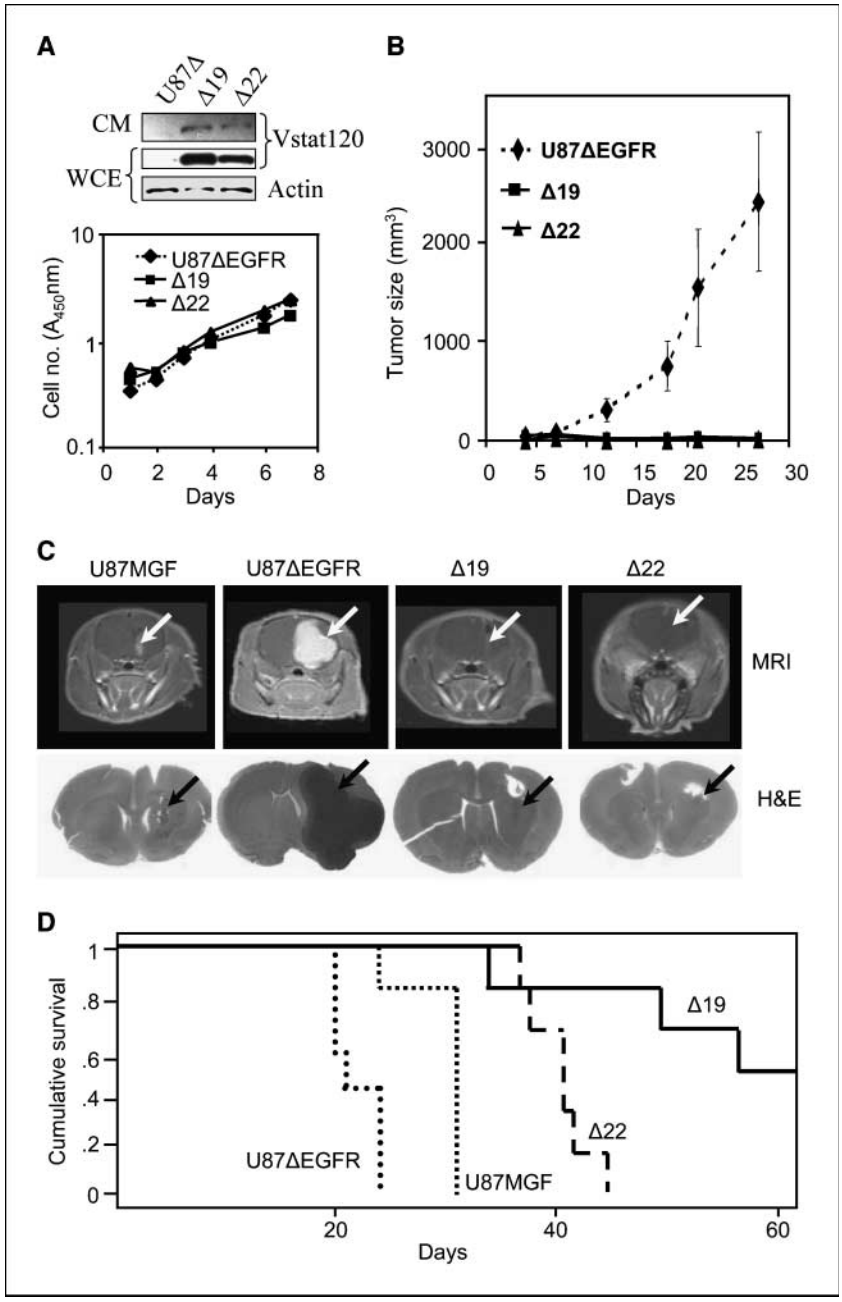

Figure 2. Vstat120 expression suppresses subcutaneous and intracranial tumor growth of U87ΔEGFR cells despite the proangiogenic stimulus provided by EGFRvIII. *A,* characterization of U87ΔEGFR and Vstat120-expressing clones Δ19 and Δ22. *Top,* Western blot analysis of whole cell extract (*WCE*) and conditioned medium (*CM*) from U87ΔEGFR cells (*U87Δ*) and derived clones Δ19 and Δ22, which stably express Vstat120. *Bottom, in vitro* proliferation rates of U87 ΔEGFR cells, and Vstat120 expressing clones Δ19 and Δ22, as measured using the crystal violet assay. Expression of Vstat120 does not alter the *in vitro* proliferation rates of these cells. *B,* subcutaneous growth of U87ΔEGFR and Vstat120-expressing clones Δ19 and Δ22 in *nu/nu* mice. U87ΔEGFR and derived clones stably expressing Vstat120 (Δ19 and Δ22) were injected s.c. into mice ($n = 6$) and the tumor volume for the indicated clones was plotted as a function of time. Note the strongly decreased tumor growth of clones expressing Vstat120. *C,* relative growth of U87MGF, U87ΔEGFR, and Vstat120-expressing clones in rat brains. *Top,* MRI scans of individual rat brains 14 d after intracranial implantation of 10^6 tumor cells. The presence of a glioma is detected through the bright areas (*white arrows*) of contrast enhancement from the MRI contrast agent (Gd-DTPA). Note the small tumor in U87MGF cells, the large tumor in U87ΔEGFR cells, and the barely detectable minimal tumors in clones Δ22 and Δ19. *Bottom,* corresponding histopathologic brain sections stained with H&E. Tumor growth is visible as a darkly stained area (*black arrow*). *D,* survival curves of rats implanted with U87MGF, U87ΔEGFR, and Vstat120-expressing clones, Δ19 and Δ22. Cells (1×10^6) were implanted stereotactically in the brain of athymic *nu/nu* rats. Rats implanted with U87ΔEGFR cells had the shortest survival time due to the very angiogenic and aggressive nature of these tumors. Vstat120-expressing clones Δ19 and Δ22 showed a significant improvement in their survival compared with the parental U87ΔEGFR and control U87MGF cells ($P < 0.05$).

U87MGD glioma cells was 18 days. In contrast, the median survival of the animals injected with Vstat120-expressing clones U14 and U18 was 28 (range, 24–34) and 41 (range, 34–49) days, respectively (Fig. 1*D*).

Expression of Vstat120 can suppress intracranial tumor growth even when a proangiogenic stimulus is present. Parental U87MGF malignant glioma cells are proangiogenic due to the loss of PTEN (32). However, they lack expression of EGFRvIII, the genetic hallmark of a large subset of GBM (10, 11). This mutation confers an aggressive and highly angiogenic phenotype (26, 33). To test if Vstat120 could suppress the growth of such highly aggressive gliomas, we used U87MGF glioma cells that stably express the EGFRvIII mutant receptor (U87ΔEGFR; ref. 26). We then stably transfected U87ΔEGFR with a Vstat120 expression vector and selected two clones (Δ19 and Δ22) for further analyses. These cells expressed Vstat120 in both the whole cell extract and conditioned medium, and did not show any alterations in their *in vitro* proliferation rates (Fig. 2*A*). To assess the therapeutic potential of Vstat120 expression on this highly aggressive glioma, we used both the mouse subcutaneous and rat orthotopic xenograft models.

Athymic *nu/nu* mice ($n = 6$/group) injected with U87ΔEGFR cells formed large subcutaneous tumors, and mice had to be sacrificed by day 25. In contrast, mice injected with Vstat120-expressing cells showed significant tumor growth suppression (Fig. 2*B*). Western blot analysis of the excised tumors revealed expression of Vstat120 *in vivo* (Supplementary Fig. S1). To examine whether Vstat120 would also antagonize tumor formation in their orthotopic

microenvironment, we implanted 10^6 cells of U87MGF, U87ΔEGFR, Δ19, and Δ22 cells stereotactically in the brain of athymic *nu/nu* rats. Initially, the effect of Vstat120 on tumor growth was measured noninvasively by MRI on day 14 to determine tumor growth (n = 3/group). Immediately thereafter, the animals were sacrificed and corresponding sections of the brains were analyzed by H&E staining. Both MRI and pathology results evidenced smaller tumors in gliomas derived from cells expressing Vstat120 (Fig. 2*C*). Next, we examined the effect of Vstat120 expression on the survival of animals with intracranial tumors (n = 6 animals/group). Consistent with previous reports (26), the added expression of EGFRvIII to U87MGF cells significantly reduced the median survival of rats from 31 to 21 days (P < 0.002). In contrast, the median survival of rats implanted with intracranial Δ19 and Δ22 cells was 57 days (34–114 days) and 41 days (37–45 days), respectively (Fig. 2*D*).

These results showed that expression of Vstat120 significantly slowed tumor growth and increased survival (P < 0.001 between animals implanted with either of the Vstat120-expressing clones, Δ19 and Δ22, and the control U87ΔEGFR cells). Interestingly, among rats injected with Vstat120-expressing Δ19 cells, there were three long-term survivors who lived for more than 60 days after tumor cell implantation. Two of these three rats eventually died of tumor burden on days 85 and 114, and the third animal was sacrificed on day 168 and found to be tumor-free. Combined, the above results show that Vstat120 has potent inhibitory effects on glioma growth *in vivo*, both in the subcutaneous and in the brain microenvironments.

Measurement of vascular density in intracranial gliomas. To determine whether the reduced ability of Vstat120-expressing cells to grow *in vivo* but not *in vitro* was due to impairment in recruiting the vascular supply needed for solid tumor growth, we examined the vascular phenotype of intracranial tumors derived from U87ΔEGFR and Vstat120 clones. Immunohistochemistry for von Willebrand factor, a vascular marker, revealed a significant reduction in the density of vascular structures in Vstat120-expressing tumors (Fig. 3*A*). Vessel density in brain tumor sections derived from Vstat120-expressing cells (Δ19 and Δ22) showed an average of 18 (± 2.0) vessels/mm^2, whereas control U87ΔEGFR tumors had 32 (±1.5) vessels/mm^2 (P < 0.005; Fig. 3*B*). These data show that Vstat120 can reduce the vascular density of a very aggressive form of human brain tumor in its orthotopic microenvironment in a rat model.

Vstat120-mediated inhibition of endothelial cell migration *in vitro* requires CD36. The above data, combined with our previous demonstration that Vstat120 inhibits endothelial cell migration *in vitro* (19), suggests that Vstat120 can suppress angiogenesis by antagonizing the neovascularization response of endothelial cells. Vstat120 contains five TSRs and an integrin-binding RGD motif, both of which are known to impart an antiangiogenic function to thrombospondins (13, 20, 21, 34). The antiangiogenic effects of TSRs found in TSP-1 are mediated primarily upon binding to CD36 on endothelial cells (35). Whether TSRs in nonthrombospondin proteins can also regulate angiogenesis through CD36 is currently unknown. Therefore, we examined if interactions with CD36 may play a mechanistic role in Vstat120's angiostatic function, likely through its five TSRs (35). CD36 is known to be strongly expressed on HDMECs, whereas very little to none is found on HUVECs (36). We confirmed the differential expression of CD36 in HDMEC and HUVEC (Fig. 4*A*). To evaluate the role played by CD36 on Vstat120 antiangiogenic effect, we compared the susceptibility of CD36-expressing HDMEC and nonexpressing HUVECs to the inhibitory effects of Vstat120 in a transwell migration assay. Treatment of endothelial cells with CM from 293 cells expressing Vstat120 (Fig. 4*B, left*) inhibited the migration of CD36-expressing HDMECs, but had no effect on CD36-nonexpressing HUVEC cell migration, potentially implicating CD36 in Vstat120 effects (Fig. 4*B, right*). The effect of Vstat120 on HDMEC migration was further tested in a scratch-wound migration assay (Fig. 4*C*). Confluent HDMECs were wounded and the extent of wound closure was measured after 8 hours, at which time, the cells were fixed and stained. The leading edge of cells

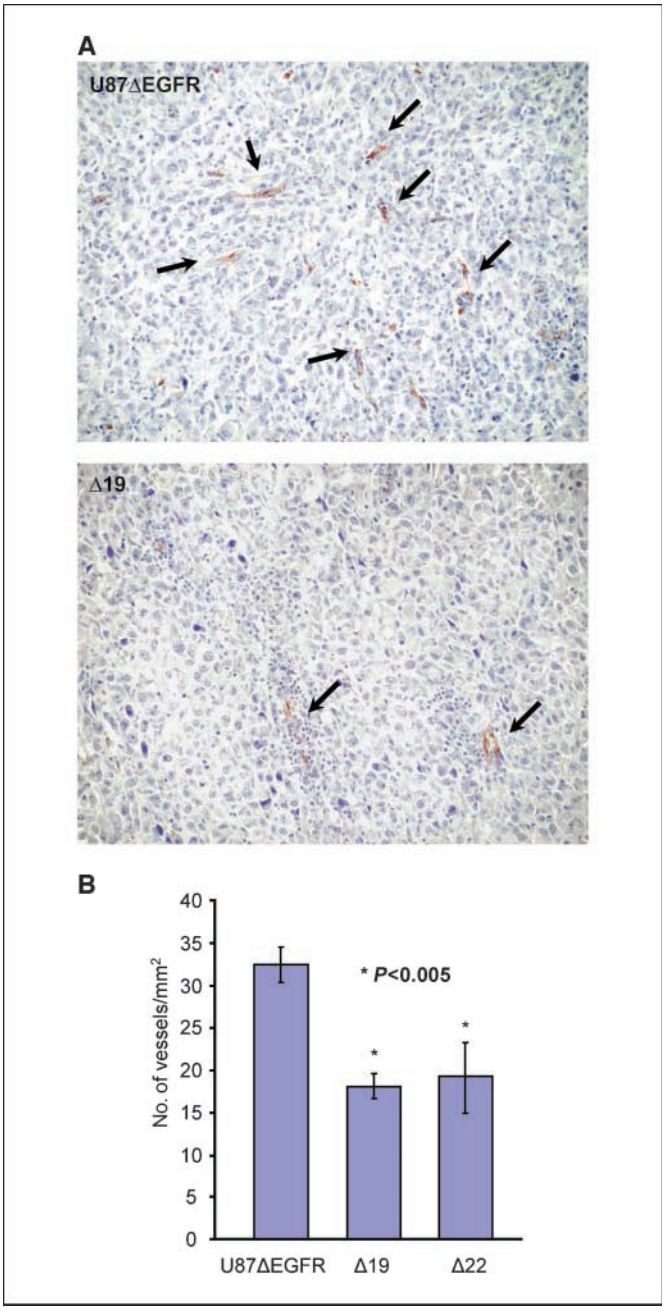

Figure 3. *In vivo* antiangiogenic effect of Vstat120 produced by glioma cells. *A,* immunohistochemistry for von Willebrand factor in tumor sections derived from U87ΔEGFR (*top*) or Vstat120-expressing clone (Δ19; *bottom*). *Brown,* endothelial cells lining capillaries (*arrows*). *B,* vessel densities in U87ΔEGFR and Vstat120-expressing clones (Δ19 and Δ22) were determined. Vstat120-expressing tumors showed significantly lower vessel density than parental tumors. *Columns,* mean vessel densities; *bars,* SE; *, P < 0.005.

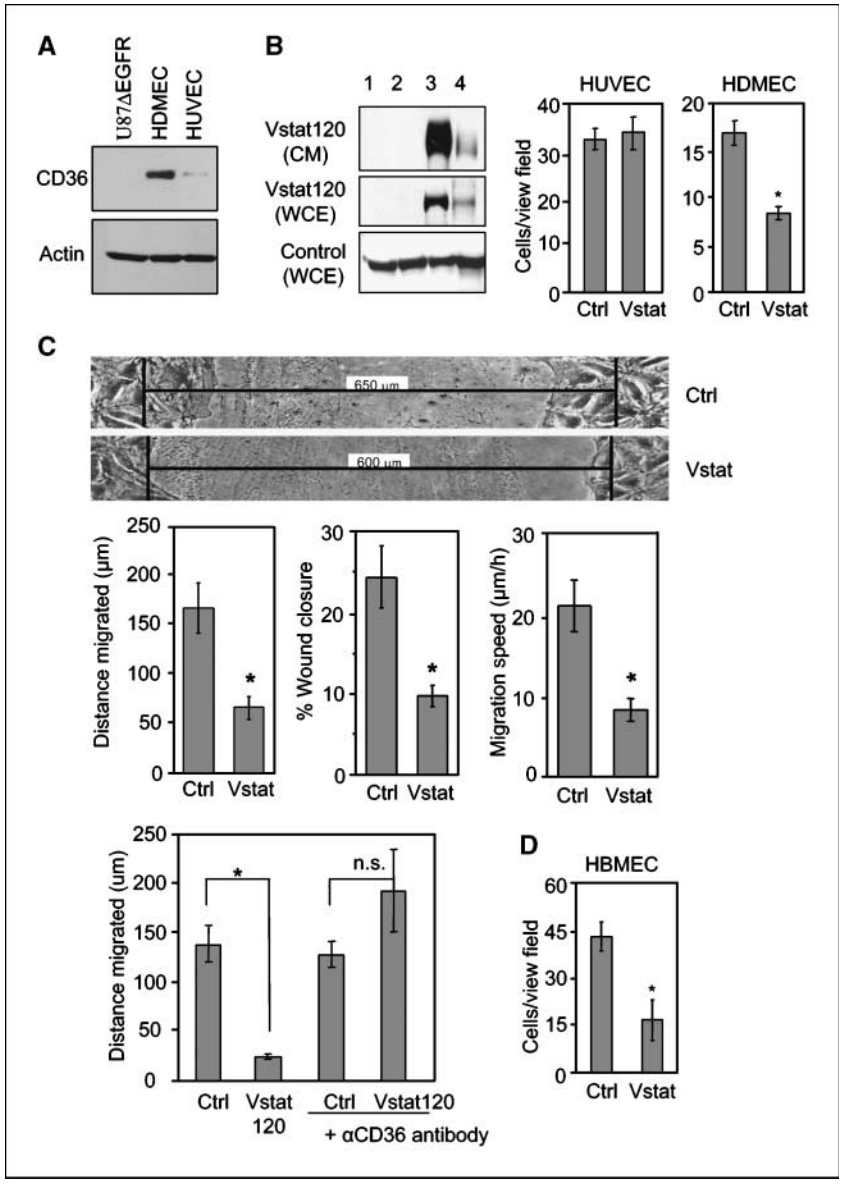

Figure 4. Vstat120 inhibits endothelial cell migration in a CD36-dependent fashion. *A,* Western blot analysis for expression of CD36 in U87ΔEGFR, HDMEC, and HUVEC cells, respectively. *B,* production of secreted Vstat120 by transient transfection in 293 cells (*left*). The cells (80% confluent) were left untreated (*lane 1*) or were transfected with either control pcDNA3.1lacZ vector (*lane 2*) or Vstat120 expression vector pcDNA3.1Vstat120-myc/his (*lane 3*). Vstat120 produced by cells transfected with full-length BAI1 expression vector was used as a size control (*lane 4*). CM was collected in serum-free medium for 48 h and used in experiments *B* to *D. WCE,* whole cell extract. *Right,* transwell migration assays examining the migration of HUVEC and HDMEC in the presence of CM from control or Vstat120-containing CM from 293 cells. The number of cells that migrated to the bottom of the chamber after 8 h was quantified as described in Materials and Methods. Note that Vstat120 containing CM reduces the migration of HDMEC, but not HUVEC. *C,* scratch-wound migration assays. Confluent HDMECs were wounded, treated with CM prepared as in *B*, and the endothelial cells allowed to migrate for 8 h, then fixed and stained with crystal violet. *Top*, representative pictures of migrated cells treated with control (*upper*) or Vstat120 CM (*lower*). *Black bars,* initial wound width in micrometers. Distance of migration, percentage of wound closure, and speed of migration were quantified (*middle*). The experiment was repeated twice with similar results. *Columns,* mean; *bars,* SE ($n = 6$ for each condition); *, $P < 0.01$ compared with Vstat120. CD36 function-blocking antibody prevents Vstat120 antiangiogenic function (*bottom*). HDMECs were wounded, then either left untreated or treated with anti-CD36 function–blocking antibody at 10 μg/mL for 30 min. The cells were next treated with CM (as above) for 30 min, followed by treatment with 10% serum to induce cell migration. Final wound width was measured after 8 h and the distance migrated was calculated. *D,* transwell assay examining the migration of HBMEC in the presence of CM from U87MGD (*Ctrl*) and Vstat120-expressing U14 cells (*Vstat*). *Columns,* mean; *bars,* SE ($n = 3$ for each condition); *, $P < 0.05$ and n.s., not significant by Student's *t* test.

migrated a greater distance in the control cells compared with the Vstat120-treated cells. Quantification of the distance migrated, percentage of wound closure, and migration speed of cells showed that Vstat120 significantly reduced the migration of HDMECs.

Next, we determined whether an anti-CD36 function–blocking antibody could abrogate the inhibitory function of Vstat120 on HDMECs in a scratch-wound migration assay (Fig. 4*C, lower panel*). Confluent HDMECs were left untreated or were treated with anti-CD36 antibody for 30 minutes prior to treatment with control or Vstat120-containing CM. Quantification of these results showed that preincubation of HDMECs with neutralizing anti-CD36 antibody completely abrogated the antimigratory effect of Vstat120. Altogether, these findings suggest that Vstat120 can antagonize the migration of endothelial cells in a CD36-dependent fashion.

To further examine whether these findings were consistent with the antitumor and antivascular effects of Vstat120 in brain, it was critical to show CD36 expression in brain tumor vasculature and that Vstat120-secreting glioma cells could inhibit the function of brain-derived endothelial cells *in vitro*. Immunofluorescent staining of normal brain (human and mouse) and human glioblastoma specimens for factor VIII and CD36 confirmed the presence of CD36 in brain and glioma vasculature (Supplementary Fig. S2, available online). Transwell assays showed that the migration of primary human brain microvascular endothelial cells (HBMEC) was blocked with CM from Vstat120-expressing U14 glioma cells *in vitro* (Fig. 4*D*).

Vstat120 can bind to the CLESH domain of CD36. The antiangiogenic effects of TSP-1 and TSP-2 are mediated by their binding to CD36 on endothelial cells. This interaction is dependent on the binding of the TSR domain(s) to a conserved region within CD36 called the CLESH domain (reviewed in ref. 37). Consequently, we tested the ability of Vstat120 to bind to recombinant CD36 CLESH domain peptides. GST-tagged peptides spanning amino acids 5 to 143 and 67 to 157 of CD36 were expressed and purified in *E. coli* (Fig. 5*A* and *B*). The indicated GST fusion proteins were tested for their ability to bind to TSP-1. Briefly, the indicated recombinant peptide bound to glutathione-sepharose beads was used to pull down TSP-1 from CM of LN229 cells constitutively

expressing TSP-1 (clone C9). Western blot of the pulled down proteins confirmed their ability to bind to TSRs. (Fig. 5*C, left*). The indicated GST fusion proteins were then tested for their ability to bind to Vstat120 in a similar pull-down assay using Vstat120 from CM of LN229 glioma cells constitutively expressing Vstat120. Figure 5*C* shows that the GST-tagged recombinant CD36 CLESH proteins, but not GST alone, pulled down Vstat120. These results show the ability of Vstat120 to bind to the CLESH domain of CD36.

Vstat120 inhibits corneal angiogenesis in a CD36-dependent fashion. To examine whether Vstat120 would also inhibit neovascularization *in vivo*, we performed corneal angiogenesis assays in mice. To further assess the involvement of CD36 in this process, we compared the effects of Vstat120 on bFGF-induced corneal angiogenesis in wild-type and CD36 knockout mice (38). Micropellets containing human bFGF and CM of 293 cells transfected with Vstat120 cDNA or a control vector were implanted into the mice cornea. The results show that Vstat120 can reduce the extent of bFGF-induced corneal neovascularization in wild-type mice (Fig. 6*A*). This inhibitory effect was completely abolished in CD36 knockout mice. The mean area of neovascularization in corneas with pellets containing Vstat120 CM was significantly decreased (40%, $P < 0.05$) as compared with those containing control CM (Fig. 6*B*). Altogether, these results show that CD36 expression is required for Vstat120 antiangiogenic effects on endothelial cells both *in vitro* and *in vivo*.

Discussion

We have previously shown that the cleaved and secreted 120 kDa Vstat120 fragment of BAI1 functions as an autonomous paracrine antiangiogenic factor (19). We now show that Vstat120 expression can prolong the life of rats bearing intracranial gliomas. This tumor-suppressive effect of Vstat120 in the brain was sustained even when glioma cells were engineered to overexpress EGFRvIII, an oncogenic mutant EGFR resulting in highly angiogenic and aggressive tumors (26). These results highlight the potential significance of harnessing Vstat120 as a therapeutic agent for the treatment of the most malignant form of glioma in humans.

Insights into the mechanism of action of bioactive molecules is critical for their development as therapeutics. The mechanism of Vstat120 angiostatic effect is poorly understood (19, 39). The extracellular domain of BAI1 includes five TSRs and an RGD integrin-interaction motif (13). TSRs were originally discovered in TSP-1, a naturally occurring potent inhibitor of angiogenesis. TSRs are approximately 60 amino acids in length and more than 180 have been identified in over 70 TSR-containing human proteins (40). The latter include proteins of diverse functions such as the ADAMTS family of metalloproteases, complement factors C6, C7, C8, and C9, the F-, R- and M-spondins, semaphorins, Unc5, heparin-binding growth-associated molecule, and BAI-1, BAI-2, and BAI-3. The degree of sequence identity between TSR within a single protein is as diverse as that found in other TSR-containing proteins, suggesting a complex evolutionary origin (41). This high level of sequence heterogeneity between TSRs within and across diverse proteins suggests that they may carry out multiple functions. Based on current knowledge, homology in function cannot be inferred, but rather needs to be tested for each individual TSR. This highlights the importance of defining the function of individual TSRs in different proteins so that structural determinants can be identified in the future that will help accelerate the design of structure-function prediction algorithms. Although at least five TSR-containing proteins, TSP-1 and TSP-2, ADAMTS-1 and ADAMTS-8, and BAI1/Vstat120 are potent inhibitors of angiogenesis, thus far, only the TSRs of TSPs have

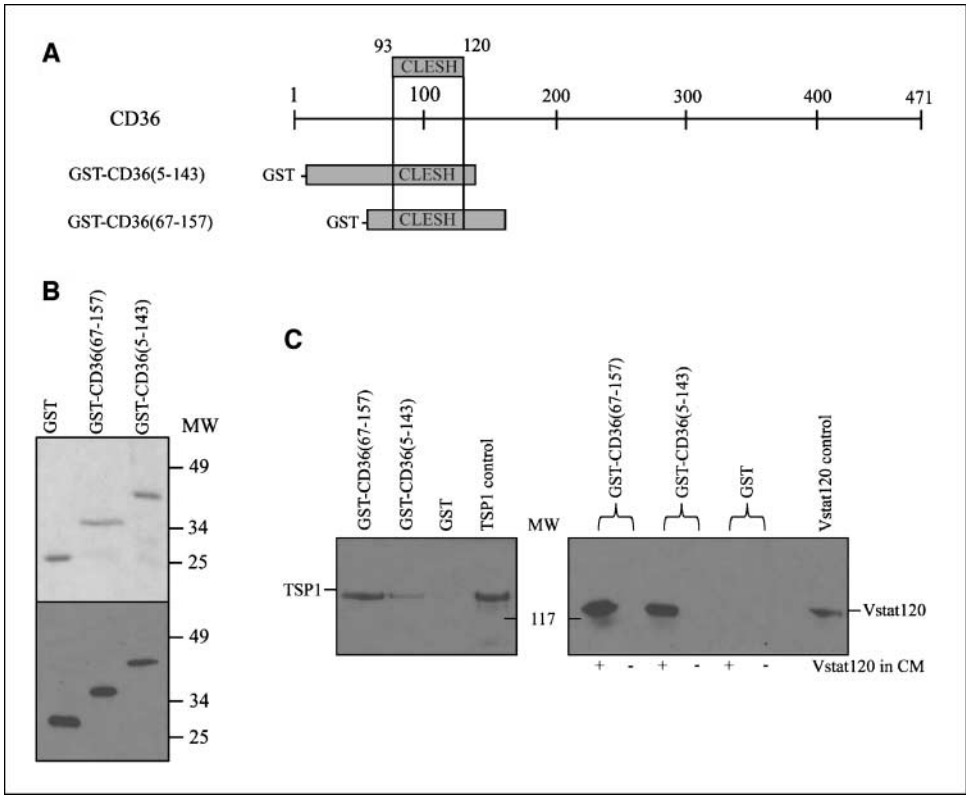

Figure 5. Vstat120 binds to the purified CLESH domain of CD36. *A,* schematic of CD36 structure with the CLESH domain. The two GST-CD36 constructs used (amino acids 5–143 and 67–157), both of which contain the CLESH domain (amino acids 93–120). *B,* Coomassie-stained gel showing purified GST (*top*), and GST-tagged recombinant proteins encoding for amino acids 67–157 and 5–143 of CD36. Proteins purified to near-homogeneity and migrated at their predicted molecular weight. Western blot analysis (*bottom*) of each fusion protein probed with anti-GST monoclonal antibody (MAB3317; Chemicon International). *C,* GST pull-down assay. GST alone or the two recombinant GST-CD36 peptides were bound to glutathione sepharose beads and CM from LN229 glioma cells stably expressing Vstat120 (+*lanes*) or control cells (– *lanes*) were tested for protein interaction. A separate pull-down assay with CM from TSP-1–expressing cells (LN229 clone C9) was used as a positive control. The bound proteins were eluted and analyzed for Vstat120 and TSP-1 expression by Western blot. Both the GST-tagged CD36-containing recombinant peptides could pull down Vstat120 and TSP-1 but not the purified GST. Positive control lanes are TCA precipitations of CM (collected serum-free after 96 h) that express either Vstat120 or TSP-1.

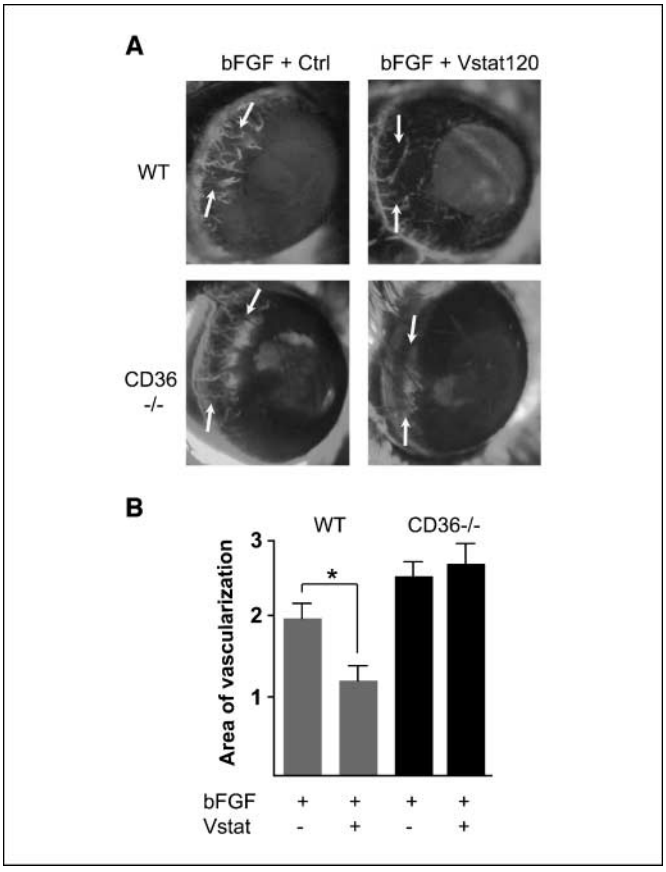

Figure 6. Vstat120 inhibits corneal angiogenesis in a CD36-dependent manner. *A,* mice cornea at 5 days postimplantation of pellets containing 25 ng of bFGF and CM of 293 cells (50 ng total CM protein) transfected with Vstat120 or vector control (*Ctrl*). FITC-dextran–labeled capillaries (*arrows*) progressing toward the pellet, previously inserted in the mouse cornea. Angiogenic response was quantified by measuring the neovascular area in the cornea. Relative to control (*top left*), CM collected from Vstat120-expressing cells (*top right*) impaired capillary formation by 40%. This effect is totally negated in CD36 knockout mice (*bottom*). The mean of neovascularized areas (mm^2) in the corneas were quantified (*B*) as described in Materials and Methods. Each condition was carried out in at least nine corneas. *Columns,* means; *bars,* SE; *, $P < 0.05$. Statistical analysis was performed using the ANOVA test.

been convincingly linked to the antiangiogenic activity of that protein family. Recent structural data have suggested that TSR-containing proteins could be subdivided into two categories based on the number and orientation of the disulfide bonds between their three antiparallel strands and the overall positive charge of their outer shell surface (42). The first category encompasses TSP-1 and TSP-2, BAI1 to BAI3, and the ADAMTS proteins, whereas the second category comprises the F-spondin and M-spondins, and some complement proteins. The fact that all known antiangiogenic TSR-containing proteins belong to the first category suggests that antiangiogenic activity might directly derive from functional homology of their TSRs. Furthermore, the likely mechanistic basis of this distinction is the capacity to bind the antiangiogenic endothelial cell receptor CD36. The studies reported here support this hypothesis, as do recent studies[7] demonstrating that recombinant TSRs from a nonangiogenic protein, F-spondin, did not bind CD36 CLESH domains.

[7] R. Simantov and R.L. Silverstein et al., unpublished results.

Purified recombinant peptides expressing three of the five TSRs in BAI1 were initially shown to inhibit angiogenesis in a rabbit corneal angiogenesis assay (13). It has remained unclear, however, whether they would serve the same function in the full-length human BAI1 protein, in which native conformation, posttranslational modifications, and physiologic concentrations might define activity. Recent data also showed that the TSRs of BAI1 are responsible for the recognition and engulfment of apoptotic cells by macrophages through the ELMO/Dock180/Rac signaling axis (43). Further complicating the issue is a recent study suggesting that the angiostatic effect of BAI1 was mediated by its ability to block $\alpha v\beta 5$ integrin receptors on endothelial cells (39). Because the antiangiogenic effects of TSP-1 and TSP-2 TSRs are mediated by their binding to CD36 and subsequent activation of a signaling cascade that triggers apoptosis (35, 38, 44), we hypothesized that the antiangiogenic effect of Vstat120 might be equally dependent on the engagement of endothelial cell CD36 by Vstat120 TSRs. Brain-derived and skin-derived endothelial cells express CD36 (44), whereas umbilical cord–derived HUVEC show very little expression (36). We first showed that Vstat120 inhibited bFGF-induced migration of CD36-expressing HDMEC and HBMECs, but not that of HUVECs. Second, we showed that the ability of Vstat120 to inhibit HDMEC migration was suppressed in the presence of function-blocking CD36 antibodies. Third, we showed that Vstat120 inhibited corneal neovascularization in wild-type but not CD36 knockout mice. Combined, our results indicate that the inhibitory effect of Vstat120 is dependent on CD36 expression on endothelial cells both *in vitro* and *in vivo*. The antiangiogenic effect mediated by TSP-1 binding to CD36 is followed by sequential activation of $p59^{fyn}$, caspase-3–like proteases and p38 mitogen-activated protein kinases, and leads to endothelial cell apoptosis (35, 38, 44). The precise signaling cascade activated by Vstat120 interaction with CD36 in endothelial cells remains to be determined, but we predict that it will likely overlap with that elicited by TSP-1 given their homology in function. If this turns out to indeed be the case, the fine structural mapping of the domains involved in TSR-CD36 interactions should facilitate the identification of critical structural requirements for binding and perhaps the development of computer algorithms to predict which TSR-containing proteins will be antiangiogenic.

The CLESH domain of CD36 (amino acids 93–120) is a critical determinant of the binding of TSP-1 and TSP-2 TSR to endothelial cells. This domain is predicted to form part of a negatively charged loop within CD36 believed to interact with the positively charged front groove of TSRs of type 1 (45, 46). We showed the ability of Vstat120 to bind to purified peptides containing the CLESH domain of CD36, indicating a specific interaction between Vstat120 and CD36, and functional homology with TSP-1 and TSP-2 TSR. These studies provide the first direct evidence that non-TSP TSRs of type 1 can bind CLESH domains.

These results show the significance of the endothelial receptor CD36 in mediating Vstat120's angiostatic effect. This is the first study showing that Vstat120 is critically dependent on the presence of CD36 to suppress the process of neovascularization both *in vitro* and *in vivo*. It remains to be determined whether Vstat120's five TSRs are sufficient, either singly or in combination, to mediate the anti-angiogenic effects of Vstat120 or whether the proximal RGD sequence is required for full activity. Synthetic peptides derived from TSP-1–derived TSRs have shown efficacy in preclinical models of cancer. ABT510 is one such peptide that has shown potent antitumorigenic effect in preclinical models and is currently being

investigated in clinical trials for safety and efficacy (44, 47, 48). Future studies are warranted to refine the minimal regions of Vstat120 necessary and sufficient to mediate its antitumorigenic functions. This can then be exploited for the development of novel anticancer therapeutic agents that can function alone or in combination with other agents such as oncolytic viruses (49, 50). Such novel agents could be Vstat peptides or peptidomimetics, or alternatively, agents that could stimulate the cleavage of endogenous BAI1 in normal brain tissue to release therapeutic doses of vasculostatin.

Disclosure of Potential Conflicts of Interest

No potential conflicts of interest were disclosed.

Acknowledgments

Received 3/31/2008; revised 8/4/2008; accepted 10/8/2008.

Grant support: NIH CA86335 (E.G. Van Meir), HL67839 (R.L. Silverstein), and NS056203 and NS059575 (B. Kaur); the National Brain Tumor Foundation and the University Research Council of Emory University (E.G. Van Meir), the American Heart Association (P.A. Klenotic), the Scott Hamilton Cares Foundation (R.L. Silverstein), and The Alex Lemonade Stand Foundation (B. Kaur). E.M. Sandberg was supported by an Emory University Cottrell Postdoctoral Fellowship. S. Cork is a graduate student in the Neuroscience program of the Emory University Graduate Division of Biological and Biomedical Sciences.

The costs of publication of this article were defrayed in part by the payment of page charges. This article must therefore be hereby marked *advertisement* in accordance with 18 U.S.C. Section 1734 solely to indicate this fact.

We thank all the lab members for helpful comments, Dr. Y. Nakamura for the BAI1 expression vector, and Drs. D. Durden, F. Furnari, and W. Cavenee for U87MG-derived glioma cells.

References

1. Folkman J. Tumor angiogenesis: therapeutic implications. N Engl J Med 1971;285:1182–6.
2. Wang D, Anderson JC, Gladson CL. The role of the extracellular matrix in angiogenesis in malignant glioma tumors. Brain Pathol 2005;15:318–26.
3. Tenan M, Fulci G, Albertoni M, et al. Thrombospondin-1 is downregulated by anoxia and suppresses tumorigenicity of human glioblastoma cells. J Exp Med 2000;191:1789–98.
4. Desbaillets I, Diserens AC, Tribolet N, Hamou MF, Van Meir EG. Upregulation of interleukin 8 by oxygen-deprived cells in glioblastoma suggests a role in leukocyte activation, chemotaxis, and angiogenesis. J Exp Med 1997;186:1201–12.
5. Batchelor TT, Sorensen AG, di Tomaso E, et al. AZD2171, a pan-VEGF receptor tyrosine kinase inhibitor, normalizes tumor vasculature and alleviates edema in glioblastoma patients. Cancer Cell 2007;11:83–95.
6. Kurozumi K, Hardcastle J, Thakur R, et al. Effect of tumor microenvironment modulation on the efficacy of oncolytic virus therapy. J Natl Cancer Inst 2007;99:1768–81.
7. Brat DJ, Castellano-Sanchez AA, Hunter SB, et al. Pseudopalisades in glioblastoma are hypoxic, express extracellular matrix proteases, and are formed by an actively migrating cell population. Cancer Res 2004;64:920–7.
8. Li J, Yen C, Liaw D, et al. PTEN, a putative protein tyrosine phosphatase gene mutated in human brain, breast, and prostate cancer. Science 1997;275:1943–7.
9. Smith JS, Tachibana I, Passe SM, et al. PTEN mutation, EGFR amplification, and outcome in patients with anaplastic astrocytoma and glioblastoma multiforme. J Natl Cancer Inst 2001;93:1246–56.
10. Ekstrand AJ, Sugawa N, James CD, Collins VP. Amplified and rearranged epidermal growth factor receptor genes in human glioblastomas reveal deletions of sequences encoding portions of the N- and/or C-terminal tails. Proc Natl Acad Sci U S A 1992;89:4309–13.
11. Libermann TA, Nusbaum HR, Razon N, et al. Amplification, enhanced expression and possible rearrangement of EGF receptor gene in primary human brain tumours of glial origin. Nature 1985;313:144–7.
12. Shiratsuchi T, Futamura M, Oda K, et al. Cloning and characterization of BAI-associated protein 1: a PDZ domain-containing protein that interacts with BAI1. Biochem Biophys Res Commun 1998;247:597–604.
13. Nishimori H, Shiratsuchi T, Urano T, et al. A novel brain-specific p53-target gene, BAI1, containing thrombospondin type 1 repeats inhibits experimental angiogenesis. Oncogene 1997;15:2145–50.
14. Kaur B, Brat DJ, Calkins CC, Van Meir EG. Brain angiogenesis inhibitor 1 is differentially expressed in normal brain and glioblastoma independently of p53 expression. Am J Pathol 2003;162:19–27.
15. Hatanaka H, Oshika Y, Abe Y, et al. Vascularization is decreased in pulmonary adenocarcinoma expressing brain-specific angiogenesis inhibitor 1 (BAI1). Int J Mol Med 2000;5:181–3.
16. Fukushima Y, Oshika Y, Tsuchida T, et al. Brain-specific angiogenesis inhibitor 1 expression is inversely correlated with vascularity and distant metastasis of colorectal cancer. Int J Oncol 1998;13:967–70.
17. Kudo S, Konda R, Obara W, et al. Inhibition of tumor growth through suppression of angiogenesis by brain-specific angiogenesis inhibitor 1 gene transfer in murine renal cell carcinoma. Oncol Rep 2007;18:785–91.
18. Kang X, Xiao X, Harata M, et al. Antiangiogenic activity of BAI1 *in vivo*: implications for gene therapy of human glioblastomas. Cancer Gene Ther 2006;13:385–92.
19. Kaur B, Brat DJ, Devi NS, Van Meir EG. Vasculostatin, a proteolytic fragment of brain angiogenesis inhibitor 1, is an antiangiogenic and antitumorigenic factor. Oncogene 2005;24:3632–42.
20. Maubant S, Saint-Dizier D, Boutillon M, et al. Blockade of αvβ3 and αvβ5 integrins by RGD mimetics induces anoikis and not integrin-mediated death in human endothelial cells. Blood 2006;108:3035–44.
21. Volpert OV, Zaichuk T, Zhou W, et al. Inducer-stimulated Fas targets activated endothelium for destruction by anti-angiogenic thrombospondin-1 and pigment epithelium-derived factor. Nat Med 2002;8:349–57.
22. Sun X, Skorstengaard K, Mosher DF. Disulfides modulate RGD-inhibitable cell adhesive activity of thrombospondin. J Cell Biol 1992;118:693–701.
23. Blouw B, Song H, Tihan T, et al. The hypoxic response of tumors is dependent on their microenvironment. Cancer Cell 2003;4:133–46.
24. Mori K, Kanemura Y, Fujikawa H, et al. Brain-specific angiogenesis inhibitor 1 (BAI1) is expressed in human cerebral neuronal cells. Neurosci Res 2002;43:69–74.
25. Ishii N, Maier D, Merlo A, et al. Frequent co-alterations of TP53, p16/CDKN2A, p14ARF, PTEN tumor suppressor genes in human glioma cell lines. Brain Pathol 1999;9:469–79.
26. Nishikawa R, Ji XD, Harmon RC, et al. A mutant epidermal growth factor receptor common in human glioma confers enhanced tumorigenicity. Proc Natl Acad Sci U S A 1994;91:7727–31.
27. Pearce SF, Roy P, Nicholson AC, et al. Recombinant glutathione S-transferase/CD36 fusion proteins define an oxidized low density lipoprotein-binding domain. J Biol Chem 1998;273:34875–81.
28. Hudziak RM, Lewis GD, Winget M, et al. p185HER2 monoclonal antibody has antiproliferative effects *in vitro* and sensitizes human breast tumor cells to tumor necrosis factor. Mol Cell Biol 1989;9:1165–72.
29. Van Meir EG. Identification of nude mice in tumorigenicity assays. Int J Cancer 1997;71:310.
30. Bowers G, He J, Schulz K, et al. Efficacy of adenoviral p53 delivery with SCH58500 in the intracranial 9l and RG2 models. Front Biosci 2003;8:a54–61.
31. Kenyon BM, Voest EE, Chen CC, et al. A model of angiogenesis in the mouse cornea. Invest Ophthalmol Vis Sci 1996;37:1625–32.
32. Wen S, Stolarov J, Myers MP, et al. PTEN controls tumor-induced angiogenesis. Proc Natl Acad Sci U S A 2001;98:4622–7.
33. Abe T, Terada K, Wakimoto H, et al. PTEN decreases *in vivo* vascularization of experimental gliomas in spite of proangiogenic stimuli. Cancer Res 2003;63:2300–5.
34. Adams JC, Lawler J. The thrombospondins. Int J Biochem Cell Biol 2004;36:961–8.
35. Dawson DW, Pearce SF, Zhong R, et al. CD36 mediates the *In vitro* inhibitory effects of thrombospondin-1 on endothelial cells. J Cell Biol 1997;138:707–17.
36. Swerlick RA, Lee KH, Wick TM, Lawley TJ. Human dermal microvascular endothelial but not human umbilical vein endothelial cells express CD36 *in vivo* and *in vitro*. J Immunol 1992;148:78–83.
37. Simantov R, Silverstein RL. Cd36: a critical anti-angiogenic receptor. Front Biosci 2003;8:S874–82.
38. Jimenez B, Volpert OV, Crawford SE, et al. Signals leading to apoptosis-dependent inhibition of neovascularization by thrombospondin-1. Nat Med 2000;6:41–8.
39. Koh JT, Kook H, Kee HJ, et al. Extracellular fragment of brain-specific angiogenesis inhibitor 1 suppresses endothelial cell proliferation by blocking αvβ5 integrin. Exp Cell Res 2004;294:172–84.
40. de Fraipont F, Nicholson AC, Feige JJ, Van Meir EG. Thrombospondins and tumor angiogenesis. Trends Mol Med 2001;7:401–7.
41. Nicholson AC, Malik SB, Logsdon JM, Jr., Van Meir EG. Functional evolution of ADAMTS genes: evidence from analyses of phylogeny and gene organization. BMC Evol Biol 2005;5:11.
42. Tan K, Duquette M, Liu JH, et al. Heparin-induced cis- and trans- dimerization modes of the thrombospondin-1 N-terminal domain. J Biol Chem 2007;283:3932–41.
43. Park D, Tosello-Trampont AC, Elliott MR, et al. BAI1 is an engulfment receptor for apoptotic cells upstream of the ELMO/Dock180/Rac module. Nature 2007;450:430–4.
44. Anderson JC, Grammer JR, Wang W, et al. ABT-510, a modified type 1 repeat peptide of thrombospondin, inhibits malignant glioma growth *in vivo* by inhibiting angiogenesis. Cancer Biol Ther 2007;6:454–62.
45. Crombie R, Silverstein RL, MacLow C, et al. Identification of a CD36-related thrombospondin 1-binding domain in HIV-1 envelope glycoprotein gp120: relationship to HIV-1-specific inhibitory factors in human saliva. J Exp Med 1998;187:25–35.
46. Crombie R, Silverstein R. Lysosomal integral membrane protein II binds thrombospondin-1. Structure-function homology with the cell adhesion molecule CD36 defines a conserved recognition motif. J Biol Chem 1998;273:4855–63.
47. Rusk A, McKeegan E, Haviv F, et al. Preclinical evaluation of antiangiogenic thrombospondin-1 peptide mimetics, ABT-526 and ABT-510, in companion dogs with naturally occurring cancers. Clin Cancer Res 2006;12:7444–55.
48. Markovic SN, Suman VJ, Rao RA, et al. A phase II study of ABT-510 (thrombospondin-1 analog) for the treatment of metastatic melanoma. Am J Clin Oncol 2007;30:303–9.
49. Kurozumi K, Hardcastle J, Thakur R, et al. Oncolytic HSV-1 infection of tumors induces angiogenesis and upregulates CYR61. Mol Ther 2008;16:1382–91.
50. Post DE, Devi NS, Li Z, et al. Cancer therapy with a replicating oncolytic adenovirus targeting the hypoxic microenvironment of tumors. Clin Cancer Res 2004;10:8603–12.